Preparation of pH-Responsive BTA@DME/PDA Microcapsules and Their Application in Anti-corrosion Coatings

Beiyao Zhang , Mingjun Zhang , Jiaying Jin , Shupei Liu , Jin song Rao , Haiyan Li *

Posted Date: 25 December 2023

doi: 10.20944/preprints202312.1873.v1

Keywords: diatomite nanoporous microcontainers; pH-responsive microcapsules; anti-corrosion coatings

Article

Preparation of pH-Responsive BTA@DME/PDA Microcapsules and Their Application in Anti-Corrosion Coatings

Beiyao Zhang [1], Mingjun Zhang [1], Jiaying Jin [1], Shupei Liu [2], Jinsong Rao [2] and Haiyan Li [1,*]

[1] Provincial Key Laboratory of Polyolefin New Materials, School of Chemistry & Chemical Engineering, Northeast Petroleum University, Daqing 163318, PR China

[2] State Key Laboratory of Mechanical Transmissions, College of Materials Science and Engineering, Chongqing University, Chongqing 400044, PR China

* Correspondence: Haiyan Li, Email address: lhy06b@163.com

Abstract: Diatomite (DME) consists of natural ordered porous structures that are excellent candidates as microcontainers. However, to the best of our knowledge, the application of DME loaded with corrosion inhibitors in anti-corrosion coatings has not hitherto been reported. In this study, DME has been used as a source of microcontainers to load benzotriazole (BTA) inhibitor by an immersion method. In order to prevent unwanted early release of the small molecule BTA inhibitor from the DME microcontainers, inspired by the adhesion characteristics of catechol and amine in mussel adhesion protein, polydopamine (PDA) was coated on their surfaces to generate BTA@DME/PDA microcapsules. Because of the depolymerization characteristics of PDA at low pH, the synthesize microcapsules showed a controllable release function. The SEM morphology, chemical structure, and loading capacity of the synthesized BTA@DME/PDA microcapsules were characterized. The corrosion resistances of epoxy coatings with different contents of BTA@DME/PDA microcapsules were compared by saline immersion and electrochemical impedance tests. A scratched coating with 5wt.% BTA@DME/PDA microcapsules showed the best anti-corrosion effect.

Keywords: diatomite nanoporous microcontainers; pH-responsive microcapsules; anti-corrosion coatings

1. Introduction

Metals are widely used in everyday' life. During the use of metal materials, they are commonly prone to corrosion due to factors such as unhindered access by air and facile damage to the material itself, resulting in functional failure [1]. Metal corrosion problems have a certain degree of impact on many aspects of daily life, and so need to be addressed urgently [2,3]. Traditional anti-corrosion methods include application of a protective layer on the surface of the substrate, but this only offers a passive barrier protection function when the coating is intact [4]. Once the coating is damaged by external stress or chemical corrosion, it will completely lose the intrinsic structure of the material and the original protection function [5,6]. Another traditional anti-corrosion method is to directly incorporate a corrosion inhibitor into the coating, prior to application on the metal surface of the metal substrate [7–9]. However, due to the detrimental effect on the curing reaction of the coating on its integrity, attempts to directly add corrosion inhibitors to improve the protective performance have met with limited access [10,11]. The idea of using nano/microcontainers to store inhibitors and embedding them into polymer matrices has been proposed, which endows the coating with self-healing and anti-corrosion abilities.

In recent years, research on microcapsules encapsulating corrosion inhibitors or healing agents has intensified [12–14]. Because of their ease of synthesis, low cost, and other advantages, it is clear that such microcapsules have great application prospects in the field of anti-corrosion [15]. At present, many nanomaterials with mesoporous structure, such as mesoporous silica and titanium dioxide, are used as micro-nano containers to encapsulate corrosion inhibitors such as benzotriazole (BTA) [16–18], and then the loaded microcapsules are incorporated into coatings to impart anti-

 doi:10.20944/preprints202312.1873.v1

corrosion properties. Diatomite (DME) is one of the important inorganic non-metallic mineral resources in China, with a large number of natural ordered porous structures [19]. The pore size is 1.7–800 nm, and the porosity is as high as 80–90%. DME can absorb 1.5–4 times its own mass of water, and tits specific surface area is 1.0–65 m^2/g [20]. DME has strong adsorption capacity, high toughness, high heat resistance, good acid resistance, and other favorable physical and chemical properties, and its cost is low [21–24]. In view of the huge reserves of natural DME, which typically has a layered porous structure, for this study, we used it instead of traditional mesoporous nanoparticles as the carrier for a coating corrosion inhibitor, which provides a new material for research in the field of anti-corrosive coatings. Spontaneous leakage and early release of corrosion inhibitors from nano/microcontainers is inevitable [25]. Therefore, there is urgent need to find a novel, simple, and green method to reduce the spontaneous leakage of low-molecular-weight inhibitors and to devise a stimulus responsive system. Many researchers have sought to apply pH-responsive films on the surface of nano/microcontainers loaded with corrosion inhibitors to obtain microcapsules showing pH-responsive release.

For this study, DME was selected as the microcontainer to carry corrosion inhibitor, and the corrosion inhibitor BTA. Considering that this low-molecular-weight inhibitor would spontaneously leak and release prematurely from the microcontainers when they are incorporated into a coating, a protective layer was applied [26,27]. Inspired by the adhesive characteristics of catechol and amine in mussel adhesion proteins [28,29], we explored the use of polydopamine (PDA) to functionalize the microcontainers in this study. PDA is formed by the self-polymerization of dopamine (DA) [30]. The synthesis conditions are very simple, making the experimental process convenient. DA is a biomolecule with adhesion and corrosion inhibitor properties, that has been widely used for surface functionalization of various materials [31–38]. When PDA-functionalized microcontainers were embedded in the epoxy coating, they showed excellent adhesion to matrix. Due to the depolymerization of PDA under acidic conditions, the microcapsules described here could be regarded as pH-responsive. When an acidic microenvironment arose in a corrosion area, PDA depolymerize and the corrosion inhibitor BTA was released from the DME. At the same time, the functional groups of PDA also formed complexes with iron oxides, which provided dual self-healing protection for metal substrate [39].

2. Experimental

2.1. Materials

BTA was purchased from Shanghai Aladdin Reagent Co., Ltd. Dopamine and Tris-hydrochloride were purchased from Suzhou Tianke Trading Co., Ltd. Anhydrous ethanol and NaOH were purchased from Tianjin Damao Chemical Reagent Co., Ltd. Diatomite (DME) was provided by Chongqing University. Epoxy and curing agent were obtained from Heilongjiang Petrochemical Research Institute. The deionized water was used in this study.

2.2. Preparation of BTA@DME/PDA microcapsules

DME was dried at 120 °C for 12 h to obtain a smooth porous structure. DME particles (1 g) were then dispersed in a 100 mg/mL solution of BTA in ethanol solution (10 mL). The obtained suspension was ultrasonically dispersed for 15 min, and was then transferred to a vacuum oven for 15 min to allow the BTA to impregnate the DME in the vacuum environment. This step was repeated three times to obtain the maximum loading of BTA. The final suspension was filtered, and the removed solid was washed several times with deionized water to remove excess BTA from the surface of the DME. Finally, the filtered sample was dried at 50 °C for 12 h to obtain the BTA@DME microcapsules.

BTA@DME microcapsules (2 g) and dopamine hydrochloride (0.4 g) were added to deionized water (80 mL). After magnetic stirring for 5 min, Tris (20 mg) was added to the suspension to initiate DA polymerization at 30 °C under magnetic stirring at 300 rpm for 24 h. The product was collected by centrifugation and filtration, and washed three times with deionized water. It was dried at 50 °C for 6 h to afford the BTA@DME/PDA microcapsules.

 doi:10.20944/preprints202312.1873.v1

2.3. Preparation of self-healing coatings

Carbon steel was used as the substrate to study the anti-corrosion properties of coatings, the surface of which was ground and cleaned before use. Different contents of BTA@DME/PDA and BTA@DME microcapsules were separately added to a mixture of epoxy and curing agent (the mass ratio of epoxy to curing agent was 3:1). The mixtures were then coated on the surface of carbon steel, and the coatings were dried in ambient air for 5 h and at 60 °C for 5 h. A pure epoxy coating was prepared by the same method without the addition of microcapsules. The dry film thickness for all coatings was about 200 μm.

2.4. Characterization

The morphology, size, and pore structure of the microcapsules and DME were observed by Scanning Electron Microscopy (SEM). The chemical structure of BTA@DME/PDA microcapsules was determined by Fourier Transform Infrared spectroscopy (FTIR) in the wavenumber range of 2000–400 cm^{-1}. The thermal stability and load capacity of the microcapsules were analyzed by Thermogravimetric Analysis (TGA) under N_2 atmosphere, heating at a rate of 10 °C/min over the range 25–600 °C. The release of BTA was monitored by UV/Vis spectrophotometry, and its absorbance at 260 nm was plotted versus time.

Th anti-corrosion properties of coatings with different microcapsule contents were evaluated by saline immersion and electrochemical impedance tests. Coating samples were scratched with a scalpel to form scratch cracks (2 cm long and 20 μm wide), and the depth of each crack was sufficient to reach the metal substrate. The scratched coating samples were soaked in 3.5 wt.% salt water for 30 days, and the corrosion phenomena at the scratched area after different number of days were observed and compared. The corrosion behavior of self-healing coatings was monitored by electrochemical impedance spectroscopy (EIS) controlled by an electrochemical workstation. A traditional three-electrode system (working electrode, saturated calomel electrode, and platinum plate electrode) was assembled in an acrylic glass tube. Four groups of samples were tested on days 3, 15 and 30 to obtain a series of Bode and Nyquist diagrams. In particular, the value of impedance modulus in the low-frequency region of the Bode diagrams were analyzed.

3. Results and discussion

3.1. SEM morphology of microcapsules

SEM images of DME are shown in Figure 1. It can be clearly seen from Figure 1 (a, b) that the pure DME consisted of disc-shaped entities of mean diameter about 30 μm with abundant pore structure on their surfaces. The hollow structure can be observed in Figure 1 (c). These pore and hollow microstructures indicated that DME was a good microcontainer for loading corrosion inhibitors and for application in anti-corrosion coatings.

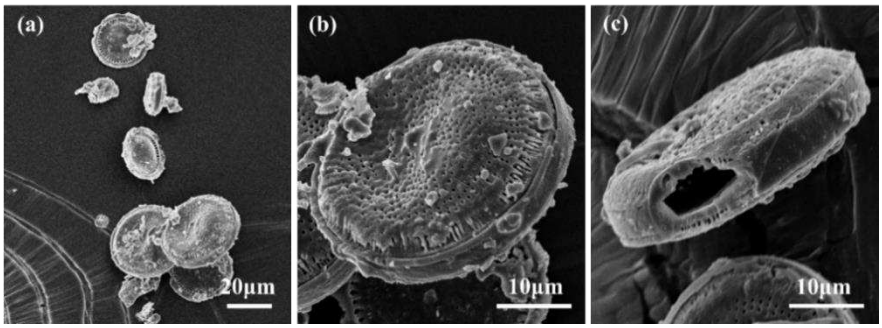

Figure 1. SEM images of DME. (a) overall morphology, (b) and (c) single amplified DME morphology.

 doi:10.20944/preprints202312.1873.v1

SEM images of BTA@DME and BTA@DME/PDA microcapsules are shown in Figure 2. It can be observed that the pore structure on the surface of DME was essentially disappears, which proves that BTA was loaded into the DMA and filling their pores as shown in Figure 2 (a). An SEM image of BTA@DME/PDA microcapsules is shown in Figure 2 (b), in which the pore structure is no longer discernible. Instead, a film layer is seen to be deposited on the outer surface of DME, due to the encapsulation by PDA.

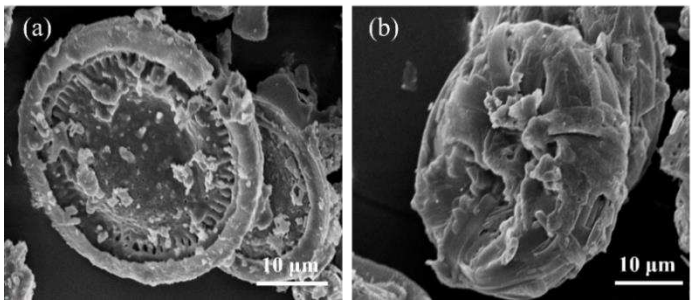

Figure 2. SEM images of (a) BTA@DME and (b) BTA@DME/PDA microcapsules.

3.2. Chemical structure of BTA@DME/PDA microcapsules

The FTIR spectra of BTA, DME, BTA@DME, and BTA@DME/PDA microcapsules are shown in Figure 3. The characteristic peaks at 789 and 1092 cm^{-1} could be attributed to an Si-O-Si symmetric stretching vibration and an Si-O asymmetric vibration, respectively, characteristic of SiO_2, the main component of DME. An absorption peak at 664 cm^{-1} could be ascribed to in-plane C-H bending vibration of the BTA benzene ring. A peak at 1456 cm^{-1} could be attributed to aromatic double bonds of the carbon skeleton, and a further peak at 1622 cm^{-1} could be ascribed to amide N-H skeleton stretching, consistent with the presence of PDA. All of these characteristic peaks could be discerned in the FTIR spectrum of the BTA@DME/PDA microcapsules, indicating that BTA was successfully loaded in the DME, which was then coated by PDA.

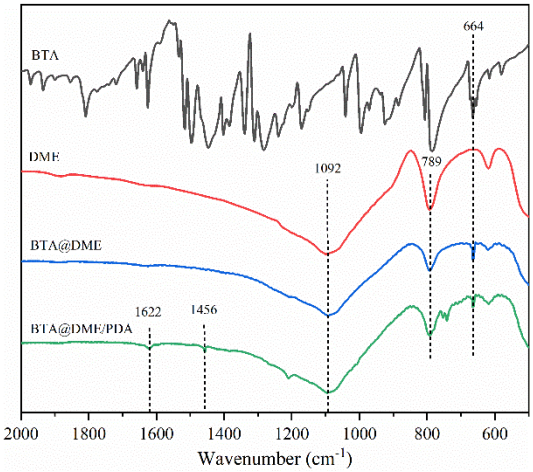

Figure 3. FTIR spectra of BTA, DME, BTA@DME microcapsules and BTA@ DME/PDA microcapsules.

3.3. Loading capacity of BTA@DME/PDA microcapsules

The loading capacity of the BTA@DME/PDA microcapsules was evaluated by TGA. Figure 4 shows TGA curves of DME, BTA and the BTA@DME/PDA microcapsules. BTA was stable below 150 °C, but was completely decomposed in the range 150–240 °C, leaving no residue. DME incurred a weight loss of about 10 wt.% during the entire heating process, 6.2 wt.% of which occurred before 240°C. The TGA curve of the BTA@DME/PDA microcapsules was thus a combination of the weight

 doi:10.20944/preprints202312.1873.v1

loss behavior of the DME microcontainers and the BTA core material. That is to say, there was a weight loss of 46.3 wt.% in the range of 150–240 °C. There was almost no further weight loss beyond 240 °C. Considering the small loss from DME, the loading capacity of the BTA@DME/PDA microcapsules must have been greater than 40%, neglecting the weight loss from the thermal degradation of a small amount of PDA. The loading capacity of BTA was thus higher than those of some mesoporous materials as nanocontainers reported in the literature. This could be mainly attributed to the abundant pores and hollow structure of DME.

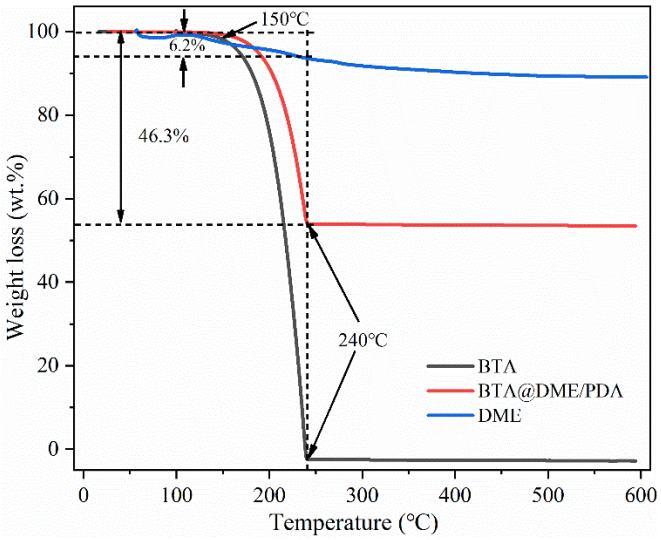

Figure 4. TG curve of BTA and BTA@DME/PDA microcapsules.

3.4. The pH responsiveness of BTA@DME/PDA microcapsules

The pH responsiveness of the BTA@DME/PDA microcapsules was analyzed by UV/Vis spectrophotometry. The release of BTA from the microcapsule samples at different pH was monitored by measuring the UV intensity at 260 nm as a function of time, as shown in Figure 5. For BTA@DME microcapsules, rapid release could be observed even under neutral conditions (pH = 7). More than 80% of the loaded BTA was released from the BTA@DME microcapsules within 200 min, implying spontaneous release due to the absence of a PDA protective layer. It is easy to imagine that when the BTA@DME microcapsules are incorporated into the coating, the BTA therein may be released prematurely, greatly reducing the corrosion inhibition effect of the coating. For the BTA@DME/PDA microcapsules, only 10% of the BTA at pH = 7 was released in the first 200 min at pH 7, and even after 600 min, little more than 10% of BTA was released, proving that the PDA film effectively inhibited spontaneous leakage of the corrosion inhibitor under neutral conditions. At pH 5 and 2, more than 50% of the BTA inhibitor was released from BTA@DME/PDA microcapsules after 200 min, and the absorbance of the solution at pH 2 was greater than that at pH 5, consistent with the results reported by Qian and Cheng etal.[16,31]. These results indicated that PDA served as an effective pH-dependent regulator valves for BTA release, its depolymerization under acidic conditions facilitated release of the loaded BTA [39].

Preprints (www.preprints.org) | NOT PEER-REVIEWED | Posted: 25 December 2023 doi:10.20944/preprints202312.1873.v1

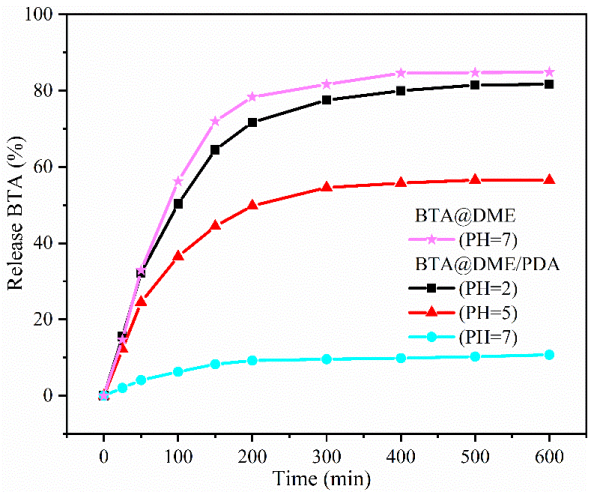

Figure 5. Release curves of BTA from BTA@DME and BTA@DME/PDA microcapsules at different pH.

3.5. Anticorrosion performance of epoxy coatings containing microcapsules

Salt solution immersion tests were performed to assess the corrosion resistances of scratched coatings. Figure 6 shows photographs of scratched epoxy coatings with different microcapsule contents after various immersion periods. It can be seen that with the extension of immersion time, the corrosion phenomena in the scratched areas of coating samples with different microcapsule contents were different. First, the corrosion resistance of a pure epoxy resin coating without microcapsules was studied, as shown in Figure 6 (a). Rust appeared on this coating sample on the third day of immersion, and the corrosion phenomenon was intensified on the 15th and 30th days. Figure 6 (b) shows photographs of the coating sample with 1 wt.% BTA@DME/PDA microcapsules. No corrosion phenomenon of the coating sample was evident on the third day of immersion, but the degree of corrosion gradually increased after the 15th day of immersion, indicating that the added 1 wt.% BTA@DME/PDA microcapsules played a certain anti-corrosion role in the initial stages, but that the anti-corrosion effect gradually weakened with the extension of immersion time. The coating samples incorporating 5 wt.% BTA@DME/PDA microcapsules showed excellent corrosion resistance throughout the immersion period, as shown in Figure 6 (c). Thus, 5 wt.% BTA@DME/PDA microcapsules imparted the coating with long-term and effective corrosion resistance. The coating sample with 10 wt.% BTA@DME/PDA microcapsules showed a certain anti-corrosion effect on the surface of carbon steel in the early stage of immersion. At the later stage of immersion, however, corrosion was rapidly aggravated. We envisage that excessive addition of microcapsules destroys the integrity of the coating matrix and weakens the interface bonding performance. Therefore, the corrosion medium can more easily penetrate the whole coating and reach the surface of the steel substrate, thereby producing more serious corrosion. In summary, the salt solution immersion test results showed that the self-healing coating with 5 wt.% BTA@DME/PDA microcapsules had the best repair performance and hence the beat corrosion protection performance for low-carbon steel.

Preprints (www.preprints.org) | NOT PEER-REVIEWED | Posted: 25 December 2023 doi:10.20944/preprints202312.1873.v1

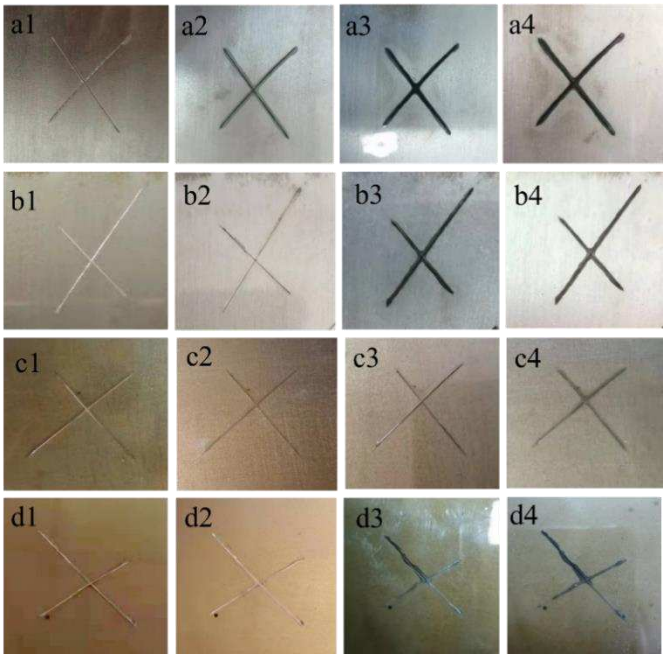

Figure 6. Optical images of epoxy coatings with different microcapsules contents (a-d: 0, 1, 5 and 10 wt. %) after immersion in 3.5 wt.% salt solution (1–4: 0, 3, 15 and 30 days).

In order to further evaluate the corrosion resistance of the coatings, electrochemical impedance tests were carried out. A pure epoxy coating without microcapsules, and epoxy coatings containing 1, 5, and 10 wt.% BTA@DME/PDA microcapsules were prepared for comparison. Scratched coatings were immersed in 3.5 wt.% aqueous NaCl solution at room temperature for 30 days, and electrochemical impedance experiments were performed at appropriate intervals. Figure 7 shows Bode and Nyquist plots for the four coatings.

Figure 7 (a_1) shows the Bode plot for a pure epoxy scratched coating. It can be seen that the impedance value of the coating at a frequency of 0.01 Hz was very low on the third day of corrosion (6366.8 Ω cm^2). With the increase of immersion time, the corrosive medium gradually penetrated into the scratches in the coating, resulting in a marked decrease in the impedance modulus of the blank coating. After 30 days of immersion, the impedance modulus at 0.01 Hz decreased to 4436.8 Ω cm^2. Figure 7 (b_1) shows the Bode plot for the coating containing 1 wt.% BTA@DME/PDA microcapsules. The impedance moduli after immersion for 3, 15, and 30 days at 0.01 Hz were 7050.5, 7314.4, and 7302.3 Ω cm^2, respectively. The overall impedance modulus was slightly higher than that of the pure epoxy coating, and there was no large fluctuation over the corrosion period. This was mainly due to the small amount of BTA inhibiting the corrosion of the coating, but the effect was not obvious. Figure 7 (c_1) shows the Bode plot for the epoxy coating containing 5 wt.% BTA@DME/PDA microcapsules. The impedance modulus at 0.01 Hz was higher than in the other cases, and continued to increase with increasing number of immersion days, rising from 18992 Ω cm^2 on day 3 to 19223 Ω cm^2 on 30 days. This corroborates that the epoxy coating with 5wt.% BTA@DME/PDA microcapsules had the best anti-corrosion effect, and that the BTA released from the nanocontainers on demand provides lasting protection for the scratched area. The amount of BTA released was sufficient to provide good corrosion resistance during the immersion period. This was mainly because, with the gradual deepening of the corrosion channels in the coating, the environment of the corrosion micro-area becomes acidic. At this time, the microcapsules incorporated in the coating showed pH responsiveness [15,38], and the BTA was released to carry out its corrosion inhibition role [40–42]. Figure7 (d_1) shows the Bode plot for corrosion of the epoxy coating containing 10 wt.% BTA@DME/PDA microcapsules. It can be seen that the overall impedance modulus at 0.01 Hz was not as high as that of the epoxy coating with 5 wt.% BTA@DME/PDA microcapsules, but was higher than those of the other three coatings. Excessive addition may destroy the integrity of the coating and

Preprints (www.preprints.org) | NOT PEER-REVIEWED | Posted: 25 December 2023 doi:10.20944/preprints202312.1873.v1

expose the steel substrate [8], further showing that the epoxy resin coating with 5wt.% BTA@DME/PDA microcapsules had the best anti-corrosion effect. Nyquist plots showed similar variations as the Bode plots. For the pure epoxy coating, as shown in Figure7 (a_2), with the extension of immersion time, the capacitance arc of steel in salt solution showed a decreasing trend. For the coatings incorporating microcapsules, as shown in Figure7 (b_2-d_2), with the extension of immersion time, the capacitive arcs showed an increasing trend. The diameter of the capacitive arc of the coating with 5wt.% BTA@DME/PDA microcapsules was the largest. These results further corroborate that the coating with 5wt.% microcapsules showed the best corrosion resistance. The equivalent circuit of the fitting curve is shown in Figure 7 (e), where RS is the solution resistance, Rc is the coating resistance, Cc is the constant phase element of the coating capacitance, R1 is the charge transfer resistance, CPE is the constant phase element of the double-layer capacitance, and R2 and CPE2 are used to describe mass transfer.

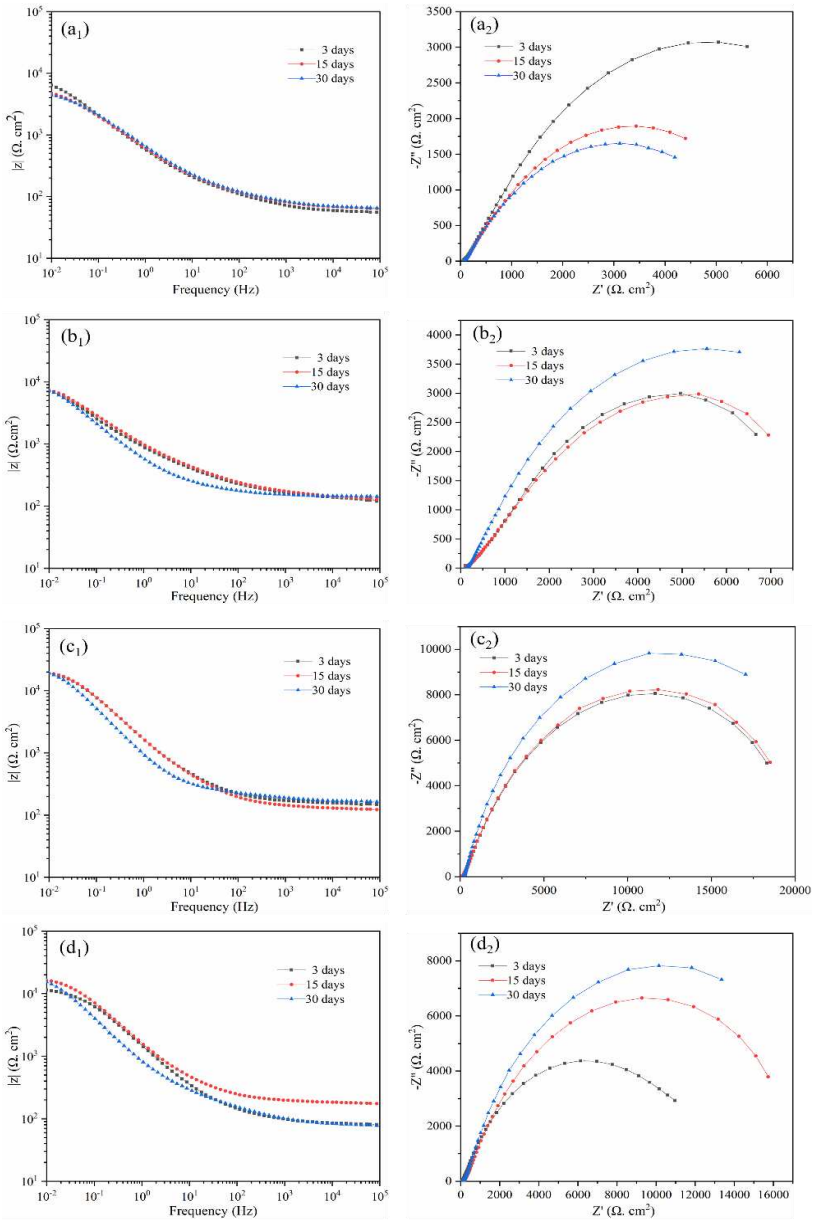

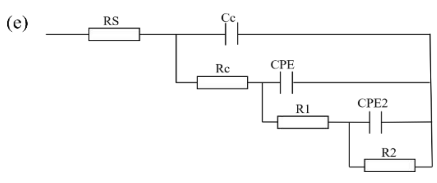

Preprints (www.preprints.org) | NOT PEER-REVIEWED | Posted: 25 December 2023 doi:10.20944/preprints202312.1873.v1

Figure 7. Bode and Nyquist curves of scratch coating with different microcapsules contents (a-d: 0, 1, 5 and 10 wt. %) after immersion in 3.5 wt.% salt solution for 30 days, (e) electrical equivalent circuit for fitting impedance data.

4. Anticorrosion mechanism of self-healing coating

Anticorrosion mechanism of self-healing coating was show in Figure 8. To avoid rapid release of the BTA inhibitor, the surfaces of the BTA@DME microcapsules were coated with PDA. Inspired by the adhesion characteristics of catechol and amine in mussel adhesion protein, the main component of DA can be oxidized and polymerized under alkaline conditions to form PDA by self-polymerization and then adsorbed onto the surface of DME, as shown in Figure 8(a). The PDA layer not only controls the release of inhibitors, as shown in Figure 8(b), but also acts as a chelating agent to form protective complexes with corrosion products. The catechol group in PDA can react with Fe^{3+} ions to form a catechol-Fe^{3+} complex [16], thereby protecting the steel matrix, as shown in Figure 8(c).

In the corrosion area of the carbon steel substrate, rust appeared around the crack, and the environment in the vicinity of the coating became an acidic micro-area. The corrosion inhibitor BTA was then released from the pH-responsive microcapsules. Under the action of the corrosion inhibitor, in the corrosion area, BTA and Fe^{2+} ions formed a protective film according to Eq. (1) to prevent further corrosion of the steel substrate [40]. In areas without corrosion, BTA could also react directly with Fe on the surface of the steel substrate, forming a protective film according to Eq. (2) [41]. The detailed anti-corrosion mechanism is shown in Figure 8 (c).

$$Fe^{2+} + 2BTA \rightarrow BTA\text{-}Fe\text{-}BTA + 2H^{+} \quad (1)$$

$$Fe + BTA \rightarrow Fe\text{-}BTA \quad (2)$$

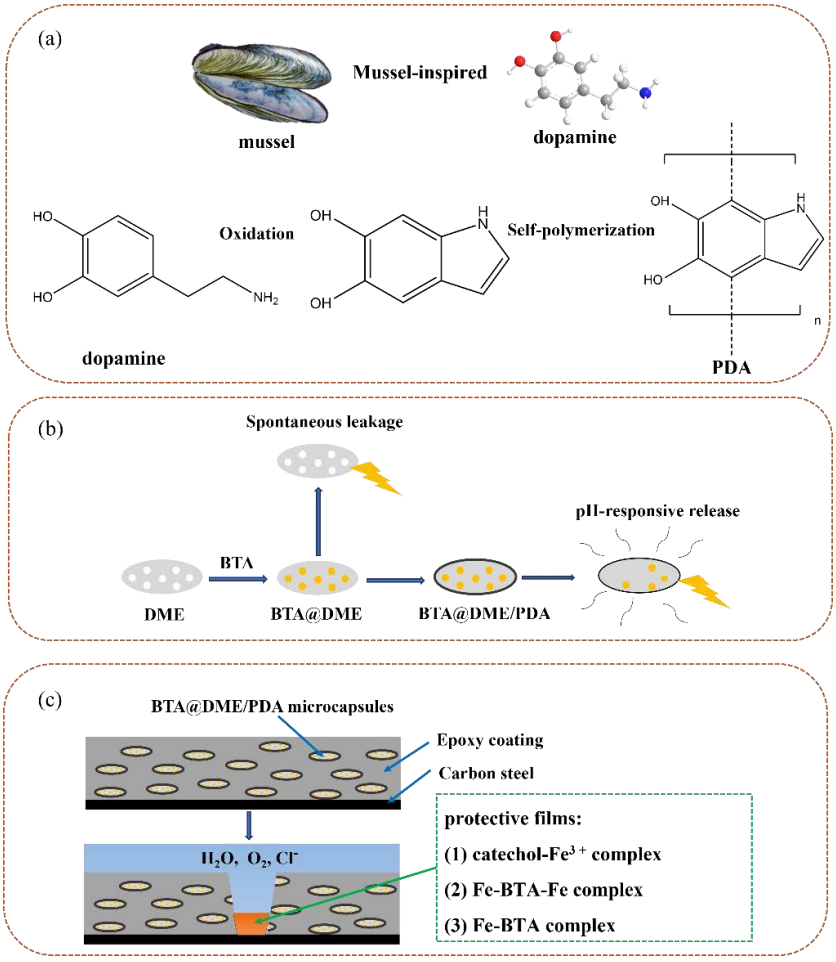

 doi:10.20944/preprints202312.1873.v1

Figure 8. Anticorrosion mechanism of self-healing coating (a) the self-polymerization of dopamine (b) pH-responsive release mechanism of microcapsules (c) proactive film form mechanism.

5. Conclusion

A self-healing anticorrosive coating containing pH-responsive microcapsules has been designed. Natural DME with a porous structure was selected as a source of microcontainers, into which BTA was loaded as a corrosion inhibitor. pH-responsive performance was achieved by applying a PDA film on the surface of BTA@DME. Self-healing anti-corrosion coatings were prepared by embedding the BTA@DME/PDA microspheres in an epoxy coating, which was uniformly applied on the surface of low-carbon steel. After immersion in 3.5 wt.% aqueous NaCl solution for 30 days, it was found that a coating with 5wt.% BTA@DME/PDA showed the best corrosion resistance and self-healing effect.

Acknowledgments: The research was financially supported by Nature Science Foundation of Heilongjiang Province (LH2023E013).

Conflicts of Interest: Authors have not a financial/commercial conflict of interest.

References

1. Cozzarini L, Marsich L, Schmid C. Ant-nest corrosion failure of heat exchangers copper pipes[J]. Engineering Failure Analysis, 2020, 109: 104387.
2. Xue S, Shen R, Chen W, et al. Corrigendum to "Corrosion fatigue failure analysis and service life prediction of high strength steel wire" [J]. Engineering Failure Analysis, 2021, 129: 105665.
3. Samiee R, Ramezanzadeh B, Mahdavian M, et al. Designing a non-hazardous nano-carrier based on graphene oxide@ Polyaniline-Praseodymium (III) for fabrication of the Active/Passive anti-corrosion coating[J]. Journal of Hazardous Materials, 2020, 398: 123136.
4. Li P, He X, Huang T C, et al. Highly effective anti-corrosion epoxy spray coatings containing self-assembled clay in smectic order[J]. Journal of Materials Chemistry A, 2015, 3(6): 2669–2676.
5. Dehghani A, Bahlakeh G, Ramezanzadeh B. Designing a novel targeted-release nano-container based on the silanized graphene oxide decorated with cerium acetylacetonate loaded beta-cyclodextrin (β-CD-CeA-MGO) for epoxy anti-corrosion coating[J]. Chemical Engineering Journal, 2020, 400: 125860.
6. Cui J, Li X, Pei Z, et al. A long-term stable and environmental friendly self-healing coating with polyaniline/sodium alginate microcapsule structure for corrosion protection of water-delivery pipelines[J]. Chemical Engineering Journal, 2019, 358: 379–388.
7. Blaiszik B J, Kramer S L B, Olugebefola S C, et al. Self-healing polymers and composites[J]. Annual review of materials research, 2010, 40(1): 179–211.
8. Shchukin D G, Möhwald H. Self-repairing coatings containing active nanoreservoirs[J]. small, 2007, 3(6): 926–943.
9. Grigoriev D, Akcakayiran D, Schenderlein M, et al. Protective organic coatings with anticorrosive and other feedback-active features: micro-and nanocontainers-based approach[J]. Corrosion, 2014, 70(5): 446–463.
10. Shchukin D G, Zheludkevich M, Yasakau K, et al. Layer-by-layer assembled nanocontainers for self-healing corrosion protection[J]. Advanced Materials, 2006, 18(13): 1672–1678.
11. Shchukin D G, Grigoriev D O, Möhwald H. Application of smart organic nanocontainers in feedback active coatings[J]. Soft Matter, 2010, 6(4): 720–725.
12. Ullah H, M Azizli K A, Man Z B, et al. The potential of microencapsulated self-healing materials for microcracks recovery in self-healing composite systems: A review[J]. Polymer reviews, 2016, 56(3): 429–485
13. Suryanarayana C, Rao K C, Kumar D. Preparation and characterization of microcapsules containing linseed oil and its use in self-healing coatings[J]. Progress in organic coatings, 2008, 63(1): 72–78.
14. Brown E N, White S R, Sottos N R. Microcapsule induced toughening in a self-healing polymer composite[J]. Journal of Materials Science, 2004, 39(5): 1703–1710.
15. Tavandashti N P, Ghorbani M, Shojaei A, et al. Inhibitor-loaded conducting polymer capsules for active corrosion protection of coating defects[J]. Corrosion Science, 2016, 112: 138–149.
16. Qian B, Zheng Z, Michailids M, et al. Mussel-inspired self-healing coatings based on polydopamine-coated nanocontainers for corrosion protection[J]. ACS applied materials & interfaces, 2019, 11(10): 10283–10291.
17. Joo J B, Zhang Q, Lee I, et al. Mesoporous anatase titania hollow nanostructures though silica-protected calcination[J]. Advanced Functional Materials, 2012, 22(1): 166–174.
18. Zheng Z, Schenderlein M, Huang X, et al. Influence of functionalization of nanocontainers on self-healing anticorrosive coatings[J]. ACS Applied Materials & Interfaces, 2015, 7(41): 22756–22766.

19. Konuklu Y, Ersoy O, Gokce O. Easy and industrially applicable impregnation process for preparation of diatomite-based phase change material nanocomposites for thermal energy storage[J]. Applied Thermal Engineering, 2015, 91: 759–766.
20. Zhang L, Zhibo H U , Sun Z , et al. Research on Diatom Mineral Content of Each Grain Size from Niger Diatomite[J]. China Powder Science and Technology, 2015.
21. Y. Noshi,A. Kobayashi,T. Uda. Model for Predicting Bathymetric and Grain Size Changes Considering Equilibrium Slopes Corresponding to Composition of Grain Size and Each Grain Size[J]. Journal of Coastal Research,2009.
22. Liu J, Zhao D F. The present situation and development of diatomite[J]. Environmental Science and Management, 2009, 34(5): 104–106.
23. Wen R, Zhang X, Huang Z, et al. Preparation and thermal properties of fatty acid/diatomite form-stable composite phase change material for thermal energy storage[J]. Solar Energy Materials and Solar Cells, 2018, 178: 273–279.
24. Rao Z, Zhang G, Xu T, et al. Experimental study on a novel form-stable phase change materials based on diatomite for solar energy storage[J]. Solar energy materials and solar cells, 2018, 182: 52–60.
25. Rao Z, Zhang G, Xu T, et al. Experimental study on a novel form-stable phase change materials based on diatomite for solar energy storage[J]. Solar energy materials and solar cells, 2018, 182: 52–60.
26. Han J, Liu S. Myristic acid-hybridized diatomite composite as a shape-stabilized phase change material for thermal energy storage[J]. RSC advances, 2017, 7(36): 22170–22177.
27. Hollamby M J, Fix D, Dönch I, et al. Hybrid polyester coating incorporating functionalized mesoporous carriers for the holistic protection of steel surfaces[J]. Advanced materials, 2011, 23(11): 1361–1365.
28. Shchukin D G. Container-based multifunctional self-healing polymer coatings[J]. Polymer Chemistry, 2013, 4(18): 4871–4877.
29. Li S, Zou Q, Li Y, et al. Smart peptide-based supramolecular photodynamic metallo-nanodrugs designed by multicomponent coordination self-assembly[J]. Journal of the American Chemical Society, 2018, 140(34): 10794–10802.
30. Ryu J H, Messersmith P B, Lee H. Polydopamine surface chemistry: a decade of discovery[J]. ACS applied materials & interfaces, 2018, 10(9): 7523–7540.
31. Cheng L, Liu C, Wu H, et al. A mussel-inspired delivery system for enhancing self-healing property of epoxy coatings[J]. Journal of Materials Science & Technology, 2021, 80: 36–49.
32. Lee H, Dellatore S M, Miller W M, et al. Mussel-inspired surface chemistry for multifunctional coatings[J]. science, 2007, 318(5849): 426–430.
33. Liu Y, Ai K, Lu L. Polydopamine and its derivative materials: synthesis and promising applications in energy, environmental, and biomedical fields[J]. Chemical reviews, 2014, 114(9): 5057–5115.
34. Lee H, Rho J, Messersmith P B. Facile conjugation of biomolecules onto surfaces via mussel adhesive protein inspired coatings[J]. Advanced materials, 2009, 21(4): 431–434.
35. Cui J, Yan Y, Such G K, et al. Immobilization and intracellular delivery of an anticancer drug using mussel-inspired polydopamine capsules[J]. Biomacromolecules, 2012, 13(8): 2225–2228.
36. Yu B, Wang D A, Ye Q, et al. Robust polydopamine nano/microcapsules and their loading and release behavior[J]. Chemical communications, 2009 (44): 6789–6791.
37. Liu X, Cao J, Li H, et al. Mussel-inspired polydopamine: a biocompatible and ultrastable coating for nanoparticles in vivo[J]. ACS nano, 2013, 7(10): 9384–9395.
38. Cheng L, Liu C, Wu H, et al. A mussel-inspired delivery system for enhancing self-healing property of epoxy coatings[J]. Journal of Materials Science & Technology, 2021, 80: 36–49.
39. Xia N N, Xiong X M, Wang J, et al. A seawater triggered dynamic coordinate bond and its application for underwater self-healing and reclaiming of lipophilic polymer[J]. Chemical science, 2016, 7(4): 2736–2742.
40. Gattinoni C, Michaelides A. Understanding corrosion inhibition with van der Waals DFT methods: the case of benzotriazole[J]. Faraday discussions, 2015, 180: 439–458.
41. Chen Z, Huang L, Zhang G, et al. Benzotriazole as a volatile corrosion inhibitor during the early stage of copper corrosion under adsorbed thin electrolyte layers[J]. Corrosion Science, 2012, 65: 214–222.
42. Cho B J, Shima S, Hamada S, et al. Investigation of cu-BTA complex formation during Cu chemical mechanical planarization process[J]. Applied Surface Science, 2016, 384: 505–510.
43. Eklund G S. Initiation of pitting at sulfide inclusions in stainless steel[J]. Journal of the Electrochemical Society, 1974, 121(4): 467.